

# 3D FINITE ELEMENT MODELING OF REINFORCED CONCRETE STRUCTURES

Helmut Hartl  
Graz University of Technology, Institute for Structural Concrete  
AUSTRIA

Christoph Handel  
Graz University of Technology, Institute for Structural Concrete  
AUSTRIA

A finite element tool based on continuum mechanics is developed for concrete with embedded 1D elements in order to represent the reinforcement and tendons. The mesh design can be achieved without considering the reinforcement layout. Rebar stiffness is integrated along its path within the parent element and no additional degrees of freedom need to be introduced for the reinforcement. Two methods accounting for slip at the interface between rebar and concrete are presented. The first method introduces a slip degree of freedom and can be addressed as a left hand approach. The second method introduces interface elements supplementary on the constitutive level, after the displacement field is computed. The effect of any kind of prestressing (initial prestressed, post-tensioned, bonded, unbonded) can be modeled easily within both methods. Concrete is modeled in terms of plasticity, with employing the Ottosen failure criterion for crushing failure. Several crack models are available for tensile failure. Creep is accounted for by integrating the entire stress history. Finally the capability of the program is shown on individual examples.

**Keywords:** 3D (three dimensional) analysis; bond slip; embedded reinforcement; finite element analysis

## 1 INTRODUCTION

A nonlinear finite element tool for reinforced and prestressed concrete structures is presented. The program is designed as a lucid analysis tool for engineers. The user has to be still experienced and cautious but he does not have to be an expert who is dealing with nonlinear finite element analyses every day. This is realized by following two key ideas: First, model the geometry of the structure as it is given in physical reality and second, employ only such material parameters which are easily accessible and understandable to an engineer.

The first idea requires that the concrete geometry is discretized correctly. Favorably, a mesh with a high regularity should be employed. The same principle applies for the reinforcement. The reinforcement should enter the model exactly at that location where it is present in nature without any restriction. Modifications of the concrete mesh or the reinforcement layout may not cause time consuming challenges. These requirements can be fulfilled employing the embedded approach, presented by Elwi [1]. Anchorage loss or even bond slip along the entire rebar can be formulated in different ways, Elwi [1], Hartl [2, 3].

Concrete failure is incorporated in terms of plasticity for its simplicity in concept. Engineers are used to this approach and to the associated parameters. Concrete crushing is modeled by the Ottosen model [4] and concrete cracking is implemented by a rotating fictitious crack model based on Hillerborg's theory [5]. Creep and shrinkage is a very important phenomenon in concrete. It is incorporated along the recommendations given in fib bulletin No 1, [6] with storing the entire stress history.

Two examples are shown. The first is a single span beam with one bonded and one unbonded tendon. It illustrates the capability of the presented slip formulation. Nonlinear concrete phenomena are not taken into account in this example. The second example investigates an existing roof girder with an unconventional cross section. Although this girder is highly prestressed, it has experienced significant deformations since the girder is very slender. The deformations are still increasing with time. The computational results are discussed and compared to the measurements on site.

The work presented here is an extension to the existing finite element program BEFE [7]. Since BEFE was initially designed for geotechnical applications, a tool for a nonlinear analysis of soil-structure interaction problems is available.

## 2 REPRESENTATION OF THE REINFORCEMENT

The mesh of the parent domain can be prepared independently of the reinforcement layout within the embedded approach. Thus, the mesh can be designed with a high regularity and a variation of the reinforcement or tendon layout does not require a modified mesh for the domain. The reinforcement needs to be provided in global coordinates only. A preprocessing routine detects automatically the intersection of the rebars with the parent element faces as shown by Hartl [2].

The integration of the stiffness matrix within the finite element framework is straightforward for the parent element. It is the first term of (2.1). Employing the embedded approach, the reinforcement stiffness is added within the same framework. The employed approach was proposed by Elwi [1] for the 2D case. The extension to the general 3D case is straightforward, Cheng [8]. The stiffness of the reinforcement is not homogeneous and isotropically distributed over the whole parent element, but available along the reinforcement only. Thus, integration for the reinforcement stiffness has to be performed along the rebar. We have to determine appropriate sample points for the numerical integration (Gauss points) along the reinforcement. The orientation of the reinforcement in this point must be computed, too. The crux in this method is that the integration points of the reinforcement need to be found in local coordinates of the parent elements. This inverse mapping is not straightforward, a Newton root finding algorithm in three dimensions needs to be applied in order to find these integration points for the rebar within the parent element.

$$\mathbf{K}^e = \int_{parent} \mathbf{B}^{eT} \mathbf{D}_c \mathbf{B}^e \cdot dV + \int_{rebar} \mathbf{B}^{eT} \mathbf{T}_{\varepsilon,gl}^T \mathbf{D}_r \mathbf{T}_{\varepsilon,gl} \mathbf{B}^e \cdot dV \quad (2.1)$$

where  $\mathbf{K}$  is the stiffness matrix,  $\mathbf{B}$  the strain displacement matrix of the parent element,  $\mathbf{D}$  the elasticity matrix of concrete or rebar and  $\mathbf{T}$  the transformation matrix of strains from the global to the local configuration of the rebar.

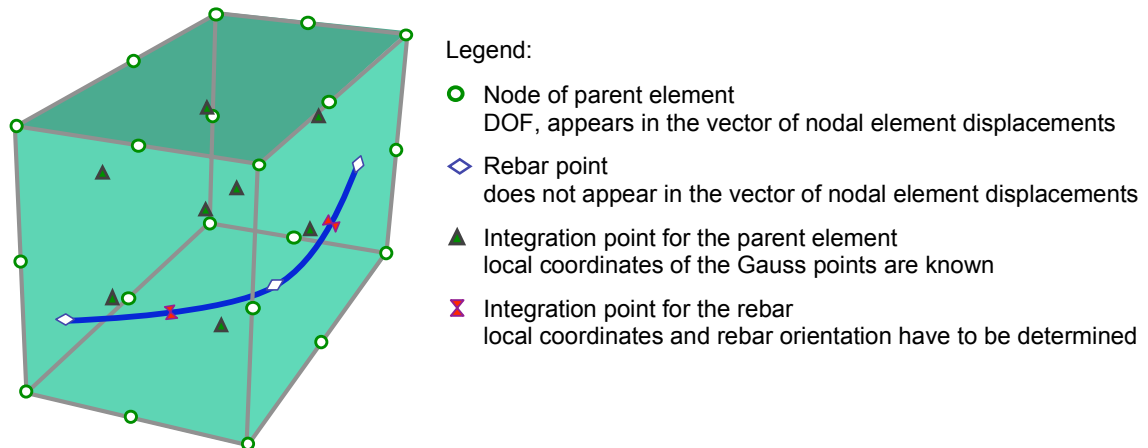


Fig. 1 Embedded reinforcement bar

Fig. 1 shows that the reinforcement is neither restricted to the parent element nodes nor it needs to be parallel to the element boundaries. It can start at any point within the parent element and it can follow a curved path as well.

### 2.1 Incorporation of bond slip

The displacement field of the parent concrete element applies for the rebar within the embedded approach as well. Thus, perfect bond is obtained. If the slip between the rebar and the concrete should be accounted for, this restriction to perfect bond needs to be relaxed.

One way is to introduce slip degrees of freedom between the parent element and the rebar. Therefore, the finite element program must offer a way to add user-defined elements, since the size of the element stiffness matrix rises for the slip degrees of freedom. Such an approach is shown below. Another way is to introduce the slip supplementary at the material level by relaxing the perfect bond restriction.

#### Embedded formulation allowing slip

This new developed form of the embedded approach allows the rebar to slip within the parent concrete element. Fig. 2 presents a brick element with parabolic shape functions and one embedded

rebar. In this special case the size of the element stiffness matrix is increased for the slip degrees of freedom from 60 to 63. The first form of this approach is presented in Elwi [1]. A new easy to follow derivation of this approach is given in Hartl [3].

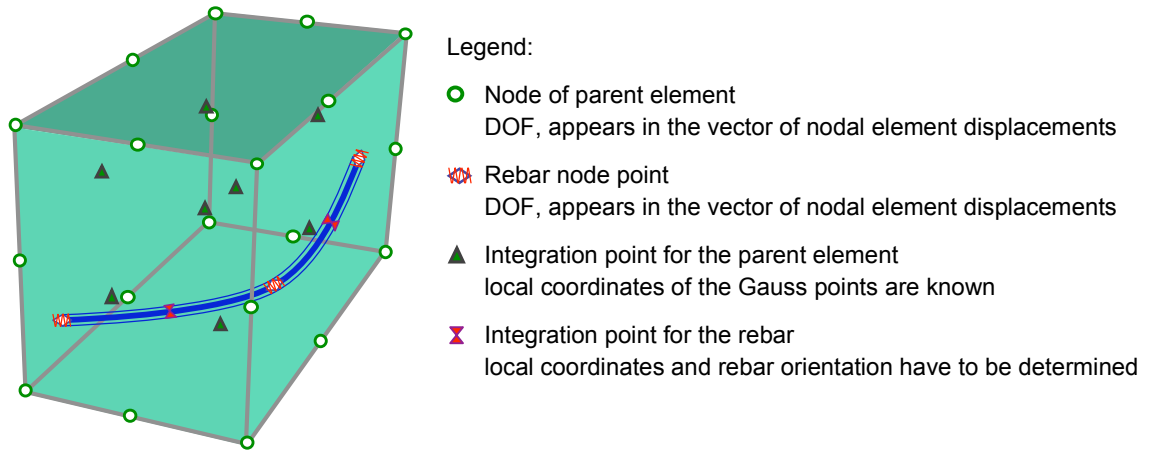


**Fig. 2** Embedded reinforcement bar allowing slip

The new introduced DOF is the slip between the concrete and the rebar. The deformation of a rebar point in terms of global coordinates is

$$\mathbf{u}_{r,g} = \begin{bmatrix} \mathbf{N} & 0 & 0 \\ 0 & \mathbf{N} & 0 \\ 0 & 0 & \mathbf{N} \end{bmatrix} \cdot \mathbf{u}_{parent}^e + \begin{bmatrix} l_1 \\ m_1 \\ n_1 \end{bmatrix} \cdot u_{slip} \quad (2.2)$$

where  $\mathbf{N}$  is the shape function matrix for the parent element nodes,  $[l_1 \ m_1 \ n_1]^T$  are the directional cosines for the rebar in the regarding rebar point and  $\mathbf{u}$  is the deformation vector. This equation can be concluded in a form such that the nodal deformations of the element and the slip deformations appear in only one vector. We can rewrite this equation in a form such that

$$\mathbf{u}_{r,g} = \begin{bmatrix} \mathbf{N} & 0 & 0 & l_1 \\ 0 & \mathbf{N} & 0 & m_1 \\ 0 & 0 & \mathbf{N} & n_1 \end{bmatrix} \cdot \mathbf{u}_{parent+slip}^e = \mathbf{H} \cdot \mathbf{u}_{parent+slip}^e \quad (2.3)$$

The internal energy of the brick element with the embedded rebar allowing slip is

$$\Delta \delta W = \int_V \delta \mathbf{u}_{parent+slip}^e \cdot \mathbf{H}^T \cdot \mathbf{B}_{truss,3D}^T \cdot E_r \cdot \mathbf{B}_{truss,3D} \cdot \mathbf{H} \cdot \Delta \mathbf{u}_{parent+slip}^e \cdot dV \quad (2.4)$$

and the stiffness matrix is

$$\mathbf{K} = \mathbf{H}^T \cdot \mathbf{B}_{truss,3D}^T \cdot E_r \cdot \mathbf{B}_{truss,3D} \cdot \mathbf{H} \quad (2.5)$$

Within this presented derivation the rebar can slide freely in the duct. An interface element can be introduced now without any difficulties between concrete and rebar. Consequently, any bond-slip situation can be modeled.

### Supplementary slip model

Interface elements are introduced supplementary on the material level after the nodal deformations have been computed by the global stiffness matrix. The concept of this so called “supplementary slip model” is shown in Fig. 3. The reinforcement is embedded in a classical way without a slip degree of freedom into the parent elements (Fig. 3a). Hence, the global analysis computes a deformation of the domain, which assumes perfect bond for the reinforcement. On the material level, this perfect bond situation is relaxed by connecting the reinforcement to the parent elements via continuous interface elements. This is illustrated by a truss analogue (Fig. 3b). The truss members are the reinforcement and the supports are represented by the parent elements. The truss elements are connected to the parent elements via bond springs, which are modeled as continuous interface elements. Yet, the strain field of the domain is integrated along the reinforcement path. The

deformation of the parent element is applied as support displacement in the truss model. A prestress force can be applied at the truss nodes, Hartl [9]. The difference in reinforcement forces computed along the truss analogue compared to forces assuming rigid bond, are mapped back as residual nodal forces of the parent element.

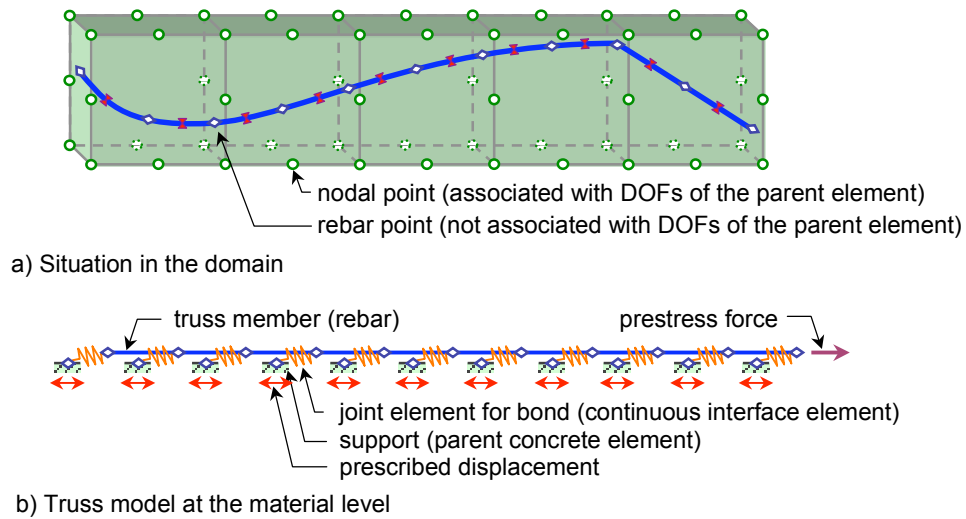


**Fig. 3** Illustration of the supplementary interface model

## 2.2 Constitutive models for the interface behavior

The constitutive model for an interface needs to be provided as a bond-stress / bond-slip diagram. Slip is the relative displacement between two associated nodes, in this case between a certain node at the rebar and the associated node in the concrete. Two constitutive models are available in the program for the interface between the reinforcement and the parent material. One is the model given in Model Code 90 [10], the other one is the Mohr-Coulomb model.

### Mohr-Coulomb interface model

Fig. 4 shows the classical Mohr-Coulomb model for frictional situations. The stress acting perpendicular to the interface can be accounted for automatically. Once the peak shear stress is reached, the shear stress is assumed to remain constant with increasing slip. This model is employed for the duct / rebar interface before the duct gets grouted. It can be applied as well for the interface between soil-anchors and the soil or the grout body. Herein, the effect of the overburden stress can be accounted for automatically, as discussed in Hartl / Pernthaler [3, 11, 12].

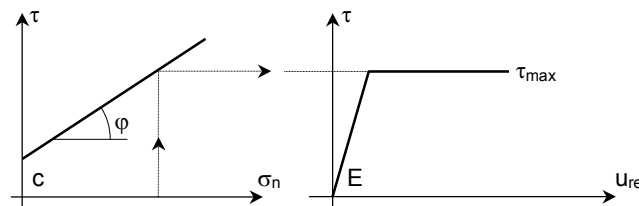


**Fig. 4** Mohr-Coulomb model (e.g. for the duct / tendon interface)

### Model Code 90 interface model

The generic shape of the bond-stress / bond-slip relation given in Model Code 90 [10] for rebars embedded in concrete is shown in Fig. 5. The model has a nonlinear ascending branch (until  $s_1$ ), an optional yield plateau ( $s_1 \div s_2$ ) at the peak shear stress ( $\tau_{max}$ ), a descending branch ( $s_2 \div s_3$ ) and a residual branch ( $\tau_{res}$ ) from  $s_3$  on. This model is employed in the program for rebars embedded in concrete and for tendons after the duct is grouted. In addition, this model can be adopted for numerous other interface situations as well.

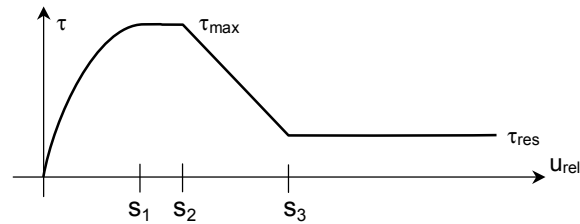


Fig. 5 Bond stress - slip diagram acc. to Model Code 90

### 2.3 Input of a rebar/tendon subjected to slip

The input of a rebar/tendon geometry as shown in Fig. 3a is straightforward. The rebar can be provided as a set of polygon points, which are independent of the concrete mesh. If a mid node is provided between two subsequent polygon points, the tendon will follow a parabolic form between these two corner nodes. The program detects the intersection points with the parent element mesh automatically in a preprocessing routine. The interface elements between rebar and concrete are also assigned automatically. Additionally, the cross sectional area, Young's modulus and the yield limit of the rebar need to be provided.

When a prestress force is applied, numerous sequences are encountered during the whole process. The prestress force can be applied in numerous load cases and each time when the hydraulic jack is removed a wedge pull in may occur. Finally, the duct may be grouted in a certain load case. All these described sequences follow generally some typical procedures. For these common procedures, the program supports the user during preparation of the input data for

- bonded tendons
- unbonded tendons
- geotechnical anchors
- initial prestressed wires

## 3 CONCRETE MODELING

### 3.1 Compressive Behavior

A linear elastic, perfectly plastic model is employed for concrete in compression. As failure surface serves the Ottosen surface [4]. The plastic potential surface is in the standard case the van Mises cylinder where no plastic volume change is obtained. Experienced users may enter a dilation angle and the van Mises Cylinder changes to a Drucker-Prager potential surface.

This approach seems to be a very crude approach for the complex behavior of concrete subjected to compressive loading at high load levels. However, it seems to be appropriate for two reasons.

First, the parameters are as simple as possible. In many cases the plastic volume change is not considered at all and the four parameters can be reduced to two following the Model Code 90 [10] recommendations, namely to the uniaxial compressive strength and to the uniaxial tensile strength. Dahl [13] gave recommendations where the four Ottosen parameters can be computed by knowing only the compressive strength. He claims that the model is able to serve as failure surface for normal and for high strength concrete with his parameters.

Second, a very accurate model for concrete under compression is not of highest importance in the authors limited opinion. It is required by design codes that failure of reinforced concrete must not be initiated by crushing of concrete. Failure has to be announced by reinforcement-yielding instead. Hence, high compressive stresses in concrete do occur very unlikely.

Concluding these two facts, a linear approximation of concrete compressive behavior within the failure surface is clear in concept and sufficient for most engineering situations. The required parameters are simple to find.

### 3.2 Tensile Behavior

Cracks are often evenly spread over tensile zones in the structure. For such cracks a smeared rotating crack model, which is based on plasticity theory, is available in this program. First the principal stresses are computed and then these principal stresses are compared to the Rankine failure surface, which is employed as failure surface and as plastic potential surface.

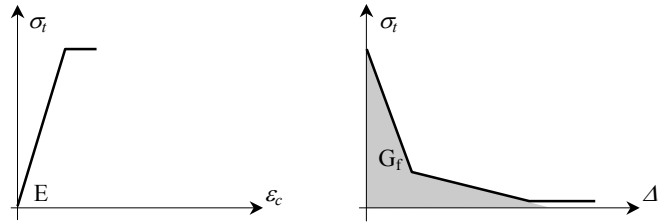


**Fig. 6** Tensile behavior of concrete

A fictitious crack model, originally proposed by Hillerborg (1976), is introduced in order to obtain results, which are independent of the element size. The pre-peak behavior and tensile yielding is formulated in a stress strain diagram. The softening regime is formulated in a bilinear stress elongation diagram, which is controlled by the crack energy and the length associated to an integration point, compare Fig. 6. This rotating crack model can be invoked as isotropic or as anisotropic model.

### 3.3 Creep and Shrinkage

Creep and shrinkage are the most important nonlinear phenomena of concrete under service load. Shrinkage is dependent on the concrete material and on the environmental conditions like moisture content and temperature. Creep is in addition to the environmental condition dependent on the stress history of the concrete. Both, creep and shrinkage is implemented along the recommendations given in fib bulletin No 1 [6]. Storing the entire stress history turned out to be no challenge for today's standard computers any more, not in concerns of memory and especially not regarding computing time. The stress history is approximated on the basis of an implicit midpoint rule as shown in Fig. 7 and in equation (3.1), (Walter (1988) [14], Hofstetter (1995) [15]).

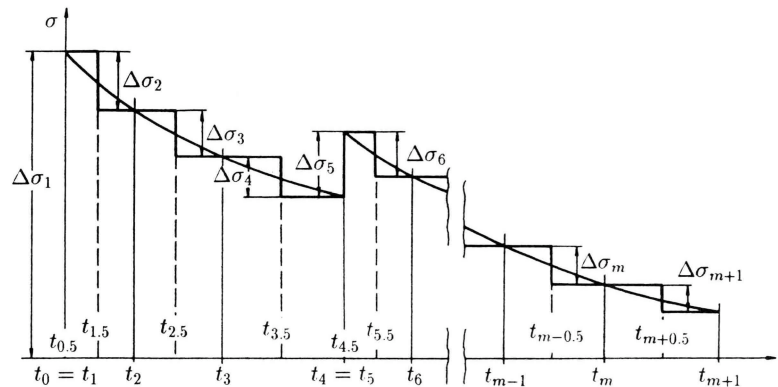


**Fig. 7** Approximation of stress history by implicit integration, [15]

$$\varepsilon^{cr} = \mathbf{A} \sum_{i=1}^m C(t_m, t_{i-1/2}) \Delta \sigma(t_i), \quad m \geq 2 \quad (3.1)$$

The program is able to assign a different history to every element. Hence, some elements can be born later than the rest of the structure. Other elements of any material type, e.g. soil, can be backfilled with concrete at a given time. However, sometimes the material parameters need to be changed without changing the history of an element. The program detects automatically the present situation and applies the right history information. Due to this storage concept it is no problem to account even for non-linear creep.

## 4 EXAMPLES

### 4.1 Beam with one post tensioned bonded and one post tensioned unbonded tendon

The example shown in this section is supposed to illustrate the performance of the supplementary slip model. The analyzed beam is shown in Fig. 8. The concrete is assumed to behave solely linear elastic and no creep and shrinkage is considered at all. Additional mild reinforcement is not taken into account as well. Hence, only the capability of the supplementary slip model is pointed out here.

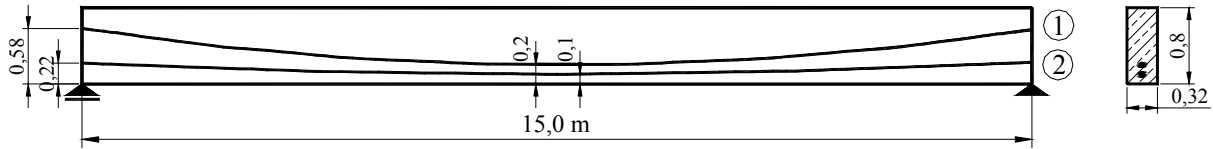


**Fig. 8** Analyzed beam

Concrete (linear elastic)  $b/h/l = 32 / 80 / 1500$  cm  $E_c = 32000\text{MN/m}^2$   $\nu = 0.20$   
 ① unbonded tendon  $A_p = 6.00\text{cm}^2$   $f_{\text{yield}} = 1385\text{MN/m}^2$   $E_p = 195000\text{MN/m}^2$   
 ② bonded tendon  $A_p = 6.00\text{cm}^2$   $f_{\text{yield}} = 1385\text{MN/m}^2$   $E_p = 195000\text{MN/m}^2$

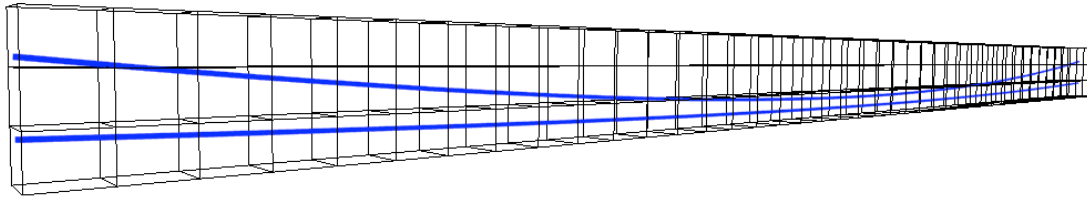


**Fig. 9** Employed mesh for the analysis

Following load cases are applied to the beam

- Load case 1: Apply a prestress force of 0.785MN to tendon ① + 50% of dead load
- Load case 2: Apply a wedge-pull-in of 1.50mm to the live anchor (left side) of tendon ①
- Load case 3: Apply a prestress force of 0.779MN to tendon ② + 50% of dead load
- Load case 4: Apply a wedge-pull-in of 1.50mm to the live anchor (left side) of tendon ②
- Load case 5: Grout the duct of tendon ② and apply a boundary load  $q=32.20\text{kN/m}$
- Load case 6: Apply an additional boundary load  $q=128.0\text{kN/m}$

The stress resulting from the loads applied are shown in Fig. 10a. The unbonded tendon 1 gets stressed in load case 1 and the Mohr-Coulomb model interface is employed for the tendon-duct interface. The cohesion is  $0.03\text{MN/m}^2$  and the friction angle is neglected. Tendon 2 is prestressed next. Load case 2 and load case 4 show the stress distribution in the tendons after the wedge-pull-in occurred. The dotted lines show the stress distribution along the rebar calculated by hand utilizing Euler's cable friction theory, where the concrete and the rebar is assumed to be rigid and the interface is assumed to behave rigid-plastic. The numerical solution is smooth since the elastic behavior of the concrete, rebar, and of the interface is taken into account as well. However, both solutions are in good agreement. Tendon 2 gets grouted in load case 5 and the Mohr-Coulomb model is replaced by the Model Code 90 model for the interface along the tendon. At the end of load case 5 the bonded tendon has started to yield, where the stress increase in the unbonded tendon at this load is comparable small as shown in Fig. 10. In load case 6 the load is increased such that the unbonded tendon starts to yield as well. The bonded tendon yields in this load case nearly along its entire path. It should be noted again, that no cracking of concrete was taken into account in this special example.

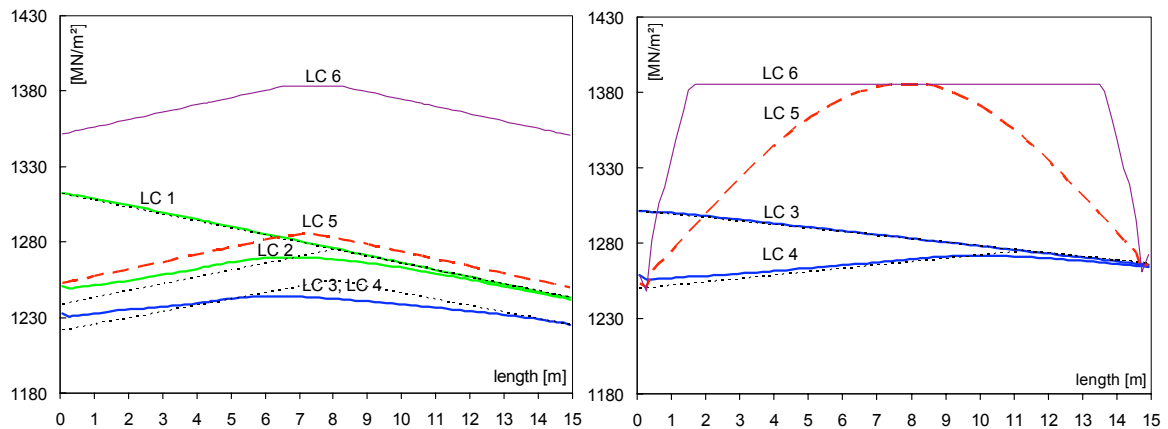


**Fig. 10 a)** Stresses in unbonded tendon ①

**b)** Stresses in bonded tendon ②

### 4.2 Roof Girder

The girder shown in Fig. 11 is a prestressed roof girder, which has a very high slenderness ratio ( $h/l \approx 26$ ). The girder was precast in three parts with concrete C40/50. On the site these three parts got supported by two temporary scaffolds. Then the joints ( $w = 17.5\text{cm}$ ) were cast with concrete C25/30. After the joint concrete had cured for 20 days at winter temperatures the tendons were introduced into the ducts and got prestressed.

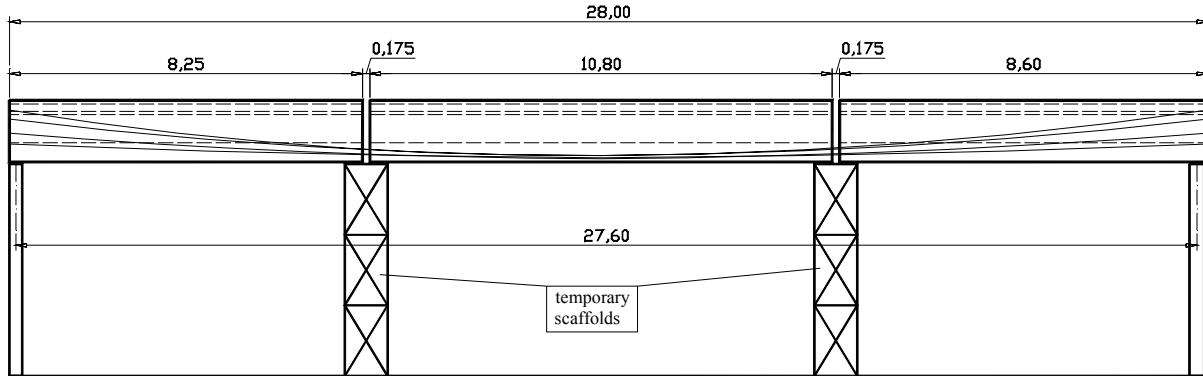


Fig. 11 Front view of the shed girder

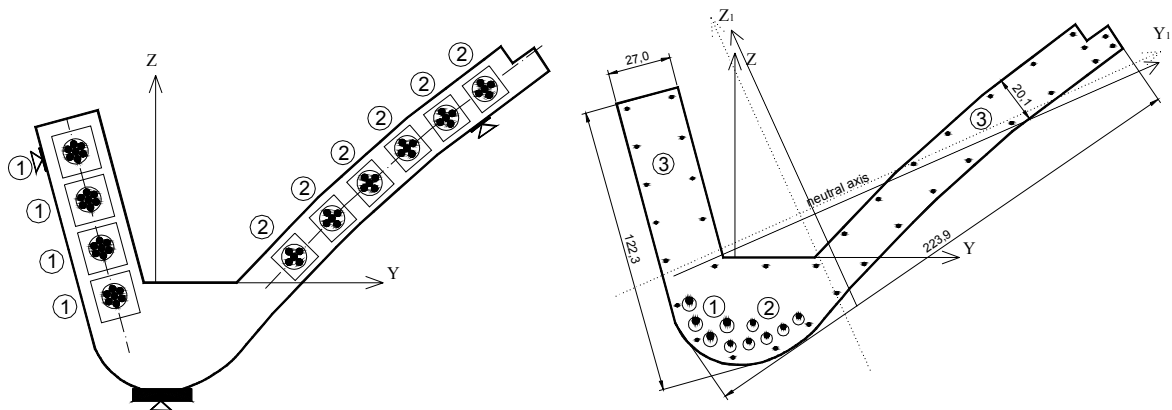


Fig. 12 a) End Cross section of the girder

b) Middle cross section of the girder

Concrete C40/50	$f_{cm} = 48\text{MN/m}^2$ , $f_{ctm} = 3.40\text{MN/m}^2$	$G_r = 90\text{Nm/m}^2$	$\nu = 0.20$	$E_c = 32000\text{MN/m}^2$
① bonded tendon (each)	$A_p = 6.00\text{cm}^2$	$f_{yk} = 1770\text{MN/m}^2$		$E_p = 190000\text{MN/m}^2$
② bonded tendon (each)	$A_p = 4.00\text{cm}^2$	$f_{yk} = 1770\text{MN/m}^2$		$E_p = 190000\text{MN/m}^2$
③ mild reinforcement (each)	$A_p = 0.79\text{cm}^2$	$f_{yk} = 500\text{MN/m}^2$		$E_p = 200000\text{MN/m}^2$

The construction process described above is accounted for in detail during the analysis. The dead load of the girder is  $19\text{kN/m}$ . The permanent load due to the roof covering is  $11.37\text{kN/m}$ . The snow load was applied accordingly to the meteorological data for this region (Salzburg/Austria). The highest snow load was  $6.46\text{kN/m}$  in winter 1999/00, when the girder was 11 years old. The snow got unloaded in this year after 30 days. Fig. 13 shows the deformation over time where the effect of creep and creep-relaxation after unloading the snow can be accounted for in a phenomenological right way, since the entire stress history is stored for the concrete. The stresses in the tendons and in the mild reinforcement can be animated by means of an internet browser at post-processing (Fig. 14). For details about the analysis of this girder reference is made to Handel [16].

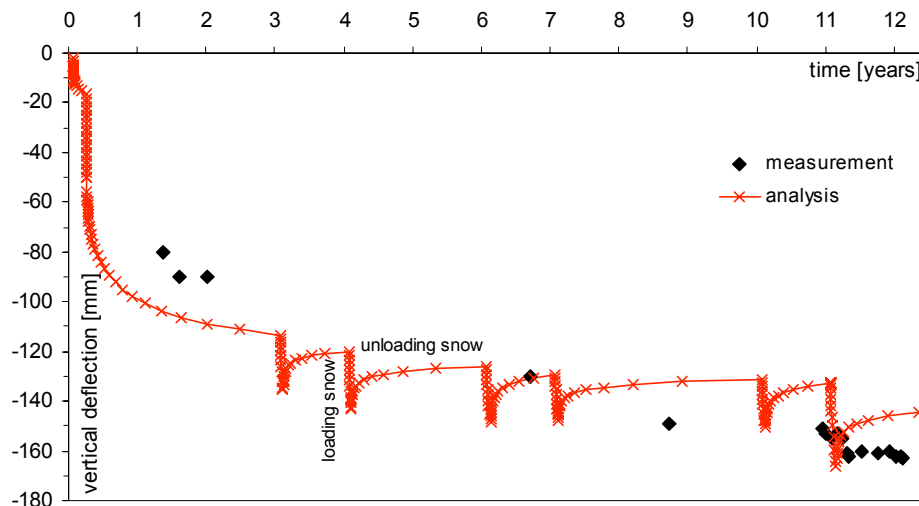


Fig. 13 Time - deformation diagram

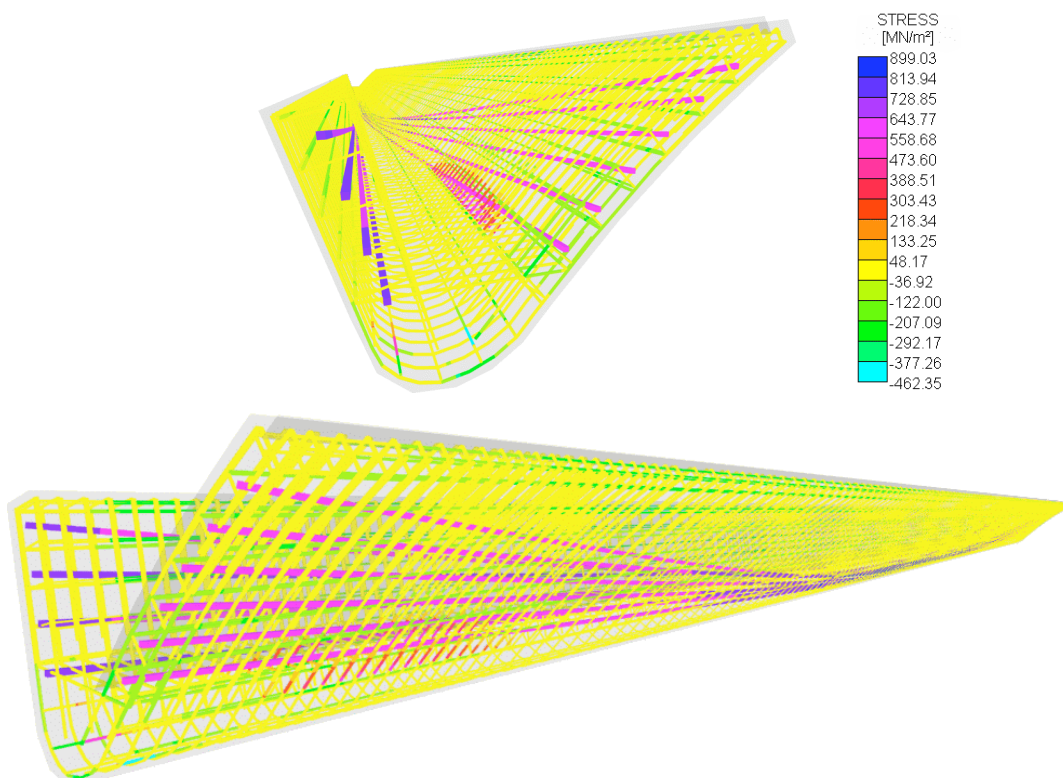


Fig. 14 Illustration of stresses in the tendons and in the mild reinforcement after 11 years

## 5 CONCLUSION & OUTLOOK

A finite element tool tailored for reinforced and prestressed concrete structures is developed. Today's standard computers are on the edge to allow such programs to become a vivid office tool for engineers, Veccio (2001) [17]. The material models are comparable simple in concept. The parameters can be obtained easily. Nevertheless, the results until now are very promising. The program is employed in teaching and for expert studies in industry with success.

Further developments are focused on two items. First, the implementation of other differential equations is a goal in order to be able to perform a coupled analysis of stress and diffusion, heat flow, etc. The second focus lies on an improved user interface.

For the current state of development reference is made to: <http://www.bau.tugraz.at/ibb/hartl>

## 6 REFERENCES

- [1] Elwi A.E., Hrudey T.M., "Finite Element Model for Curved Embedded Reinforcement", *Journal of Engineering Mechanics*, ASCE, 115, pp. 740-754, 1989
- [2] Hartl H., Sparowitz L., Elgamal A., "The 3D computational Modeling of Reinforced and Prestressed Concrete Structures", Bergmeister K. (ed.), *Proceedings of the 3rd International PhD Symposium in Civil Engineering*, Vienna, vol. 2, pp 69-79, 2000
- [3] Hartl H., "Development of a Continuum-Mechanics-Based Tool for 3D Finite Element Analysis of Reinforced Concrete Structures and Application to Problems of Soil-Structure Interaction", *Doctoral Thesis*, Graz University of Technology, 2002
- [4] Ottosen N.S., "A Failure Criterion for Concrete", *Journal of the Engineering Mechanics Division*, ASCE, 103, pp. 527-535, 1977
- [5] Hillerborg A., Modéer M., Peterson P.E., "Analysis of Crack Formation and Crack Growth in Concrete by Means of Fracture Mechanics and Finite Elements", *Cement and Concrete Research*, 6, pp 773-782, 1976
- [6] Fédération internationale du béton: fib bulletin No 1, "Structural Concrete", vol. 1, 1999
- [7] Beer G., "BEFE user's, reference & verification manual", CSS, Graz, 2001
- [8] Cheng Y.M., Fan Y., "Modeling of reinforcement in concrete and reinforcement confinement coefficient", *Finite Elements in Analysis and Design*, Elsevier, 13, pp. 271-284, 1993
- [9] Hartl H., Elgamal A., "Nicht lineare kontinuumsmechanische Modellierung vorgespannter Konstruktionen (Non Linear Modeling of Prestressed Structures based on a Continuum Mechanics Approach)" (in English), Heft 45, Österreichische Vereinigung für Beton- und Bautechnik, Vienna, pp. 87-96, 2000
- [10] CEB-FIP Comité Euro-International du Béton, "CEB-FIP Model Code 1990", London, Thomas Telford, 1993
- [11] Hartl H., Pernthaler M., "Soil anchors modeled by an embedded formulation allowing slip", *Proceedings of the second international conference on soil structure interaction in urban civil engineering*, COST Action C7, Institute for Geotechnical Engineering, Swiss Federal Institute of Technology Zurich, Zurich, pp. 123-128, 2002
- [12] Pernthaler M., "Interaktion von Schlitzwand und Baugrund unter Berücksichtigung der Nichtlinearität der Betonkonstruktionen", *Diploma Thesis*, Institute for Structural Concrete, TU-Graz, Graz, 2002 (in German)
- [13] Dahl K.K.B., "A failure criterion for normal and high strength concrete", *Technical University of Denmark*, 1992
- [14] Walter H., "Finite Elemente Berechnungen von Flächentragwerken aus Stahl- und Spannbeton unter Berücksichtigung von Langzeitverformungen und Zustand II", *Doctoral Thesis*, Technical University of Vienna, Vienna, 1998
- [15] Hofstetter, G., Mang, H.A., "Computational Mechanics of Reinforced Concrete Structures", Wiesbaden, Vieweg, 1995
- [16] Handel, Ch., "Traglastberechnung für ein schalenförmiges Sheddach", *Diploma Thesis*, Institute for Structural Concrete, TU-Graz, Graz, 2002 (in German)
- [17] Veccio F.J., "Non-linear finite element analysis of reinforced concrete: at the crossroads?", *Structural Concrete*, *Journal of the fib*, 2, No 4, pp. 201-212, 2001